



Royal Netherlands Institute for Sea Research

This is a pre-copyedited, author-produced version of an article accepted for publication, following peer review.

Ardiningsih, I.; Krisch, S.; Lodeiro, P.; Reichart, G.-J.; Achterberg, E.P.; Gledhill, M.; Middag, R. & Gerringa, L.J.A. (2020). Natural Fe-binding organic ligands in Fram Strait and over the northeast Greenland shelf. *Marine Chemistry*, 224, 103815

Published version: <https://dx.doi.org/10.1016/j.marchem.2020.103815>

NIOZ Repository: <http://imis.nioz.nl/imis.php?module=ref&refid=328453>

Research data: <https://doi.org/10.25850/nioz/7b.b.u>

[Article begins on next page]

The NIOZ Repository gives free access to the digital collection of the work of the Royal Netherlands Institute for Sea Research. This archive is managed according to the principles of the [Open Access Movement](#), and the [Open Archive Initiative](#). Each publication should be cited to its original source - please use the reference as presented.

When using parts of, or whole publications in your own work, permission from the author(s) or copyright holder(s) is always needed.

1 Natural Fe-binding organic ligands in Fram Strait and over the northeast Greenland 2 shelf

3 Indah Ardiningsih¹, Stephan Krisch², Pablo Lodeiro², Gert-Jan Reichart^{1,3}, Eric P.
4 Achterberg², Martha Gledhill², Rob Middag¹, Loes J.A. Gerringa¹

- 5 1. Royal Netherlands Institute for Sea Research (NIOZ), PO Box 59, 1790 AB Den
6 Burg, Department of Ocean Systems, University of Utrecht, the Netherlands
- 7 2. GEOMAR Helmholtz Centre for Ocean Research Kiel, Wischhofstr.1-3, 24148 Kiel,
8 Germany
- 9 3. Earth and Geoscience Department, University of Utrecht, Utrecht, the Netherlands

10
11 There is a paucity of data on Fe-binding ligands in the Arctic Ocean. Here we investigate the
12 distribution and chemical properties of natural Fe-binding ligands in Fram Strait and over the
13 northeast Greenland shelf, shedding light on their potential sources and transport. Our results
14 indicate that the main sources of organic ligands to surface waters of Fram Strait included
15 primary productivity and supply from the Arctic Ocean. We calculated the mean total Fe-
16 binding ligand concentration, $[L_t]$, in Polar Surface Water from the western Fram Strait to be
17 1.65 ± 0.4 nM eq. Fe. This value is in between reported values for the Arctic and North Atlantic
18 Oceans, confirming reports of north to south decreases in $[L_t]$ from the Arctic Ocean. The
19 differences between ligand sources in different biogeochemical provinces, resulted in
20 distinctive ligand properties and distributions that are reflected in $[L_t]$, binding strength (\log
21 K'_{FeL}) and competing strength ($\log \alpha_{FeL}$) of ligands. Higher $[L_t]$ was present near the
22 Nioghalvfjerdingsfjorden (79N) Glacier terminus and in the Westwind Trough (median of $[L_t]$ =
23 2.17 nM eq. Fe; $\log K'_{FeL} = 12.3$; $\log \alpha_{FeL} = 3.4$) than in the Norske Trough (median of $[L_t]$ =
24 1.89 nM eq. Fe; $\log K'_{FeL} = 12.8$; $\log \alpha_{FeL} = 3.8$) and in Fram Strait (median of $[L_t]$ = 1.38 nM
25 eq. Fe; $\log K'_{FeL} = 13$; $\log \alpha_{FeL} = 3.9$). However, organic ligands near the 79N Glacier terminus
26 and in the Westwind Trough were weaker, and therefore less reactive than organic ligands in
27 the Norske Trough and in Fram Strait. These weaker ligands, although more abundant than in
28 the Fram Strait, reduce overall Fe solubility in waters transported from the 79N Glacier to Fram
29 Strait. The lower ligand binding strength in the outflow results in a higher inorganic Fe
30 concentration, $[Fe^{\prime}]$, which is more prone to precipitation and/or scavenging than Fe complexed
31 with stronger ligands. Ongoing changes in the Arctic and sub-Arctic Oceans will influence both
32 terrestrially derived and *in-situ* produced Fe-binding ligands, and therefore will have
33 consequences for Fe solubility and availability to microbial populations and Fe cycling in Fram
34 Strait.

35 **Introduction**

36 The Arctic region is undergoing rapid environmental changes (Gascard et al., 2008; IPCC,
37 2014), including permafrost (Schuur et al., 2015) and ice-sheet melt (Ekwurzel et al., 2001).
38 The environmental alteration induced by climate changes will influence the biogeochemical
39 cycle of many elements, including iron (Fe), an important micronutrient regulating the
40 dynamics of primary productivity (Boyd et al., 2000; De Baar, 1990; Martin and Fitzwater,
41 1988; Rijkenberg et al., 2018). In the shelf-dominated Arctic Ocean, the Polar Surface Water
42 (PSW) is strongly influenced by runoff from Eurasian rivers with waters reaching the central
43 basin via the Transpolar Drift (TPD) (Gascard et al., 2008; Gordienko and Laktionov, 1969),
44 and lateral transport over the shelf areas. The runoff introduces organic matter, fluvial sediment,
45 and other terrigenous materials (Ekwurzel et al., 2001; Klunder et al., 2012; Measures, 1999).
46 These materials contribute organic ligands of terrestrial origin, mainly humics (Laglera et al.,
47 2019a; Slagter et al., 2019). The organic ligands stabilize Fe in the dissolved form, and prevent
48 Fe from precipitating (Kuma et al., 1996; Millero et al., 2002), thereby enabling a substantial
49 amount of dissolved-Fe (DFe) to be present in PSW (Klunder et al., 2012; Rijkenberg et al.,
50 2018; Slagter et al., 2017). Determining the complexation of Fe with organic ligands is, thus, a
51 crucial component of Fe biogeochemistry. The PSW, enriched in DFe bound to terrestrially
52 derived organic ligands as well as ligands produced in the Arctic Ocean, can be transported out
53 of the central Arctic via Fram Strait (Laukert et al., 2017; Slagter et al., 2019), a main gateway
54 for heat and water mass exchange between the Arctic Ocean and the Nordic Seas (Greenland
55 Sea, Norwegian Sea and Iceland Sea) (Rudels et al., 2005; Rudels et al., 2015). In the vicinity
56 of Fram Strait, the Nioghalvfjerdingsfjorden (79N) Glacier terminates on the northeast Greenland
57 shelf, where the Norske Trough and Westwind Trough are located. The ongoing changes in the
58 Arctic and sub-Arctic Oceans will influence the sources of Fe-binding organic ligands, and
59 therefore have consequences for DFe supply and transport, particularly in Fram Strait.
60 However, there is a paucity of data to comprehensively assess the effect of global climate
61 change on the biogeochemical cycle of DFe as well as associated feedback mechanisms.

62 Iron is present at sub-nanomolar levels in oceanic water due to its low solubility and low supply
63 rate (Liu and Millero, 2002), limiting primary productivity in approximately one third of the
64 global ocean (Boyd et al., 2000; De Baar, 1990; Martin and Fitzwater, 1988; Rijkenberg et al.,
65 2018). In seawater, DFe can exist in two different oxidation states, Fe(II) and Fe(III). The
66 Fe(III) oxidation state dominates the chemical speciation of DFe around pH 8 in oxygenated
67 waters, forming Fe oxy-hydroxides (Kuma et al., 1996). At the natural seawater pH, Fe oxy-

68 hydroxides tend to undergo further hydrolysis, and are thus prone to precipitation. However,
69 organic complexation by Fe-binding ligands shifts the equilibrium reaction away from Fe
70 hydrolysis (Kuma et al., 1996; Millero et al., 2002), governing Fe solubility in seawater
71 (Gledhill and Buck, 2012; Hunter and Boyd, 2007). Despite its importance in determining Fe
72 solubility, Fe-binding ligand data is scarce, notably in ice-covered Arctic and subarctic regions.

73 To date, only a few studies have looked at Fe-binding ligands in the subarctic and Arctic Ocean.
74 Thuróczy et al. (2011) presented the first dataset on Fe fractionation and organic chelation in
75 the central Arctic. Recently, the terrestrial influence on organic ligands in surface waters of the
76 Arctic Ocean was investigated (Slagter et al., 2017). The high concentrations of DFe (up to 4.4
77 nM) in PSW (Klunder et al., 2012; Rijkenberg et al., 2018) were facilitated by complexation
78 with enhanced concentrations of organic ligands (Slagter et al., 2017). This surface DFe
79 enhancement was a clear indication of a riverine contribution in the flow path of the TPD in the
80 Arctic Ocean. The DFe and Fe-binding ligand concentrations were up to 4.5 and 1.7 times
81 higher inside than outside the flow of the TPD, respectively, and ligands from terrestrial origin
82 dominated the total ligand pool in the TPD (Laglera et al., 2019a). This indicates a transport of
83 organic Fe-binding ligands via the TPD (Slagter et al., 2019), and these ligands are likely
84 transported out of the Arctic Ocean towards Fram Strait.

85 The concentrations and conditional stability constants (K'_{FeL}) of Fe-binding ligands in seawater
86 are typically determined by the electrochemical technique known as competitive ligand
87 equilibration (CLE) – adsorptive cathodic stripping voltammetry (AdCSV). This technique is
88 based on the competitive equilibrium between an added known ligand and natural ligands
89 present in seawater (Abualhaija and van den Berg, 2014; Croot and Johansson, 2000; Gledhill
90 and van den Berg, 1994; Rue and Bruland, 1995; van den Berg, 2006). A distribution of
91 conditional stability constants is commonly used to classify Fe-binding ligand groups (Gledhill
92 and Buck, 2012), although the boundaries between the groups are still indistinct and probably
93 more gradual than first assumed. In short, three key groups are acknowledged, (i) strong Fe-
94 binding siderophores (Mawji et al., 2008; Velasquez et al., 2016; Vraspir and Butler, 2009), (ii)
95 relatively weak Fe-binding humic substances (Bundy et al., 2014; Laglera and van den Berg,
96 2009), and (iii) relatively weak Fe-binding microbially-excreted sugars such as polysaccharides
97 or exopolymeric substances (Hassler et al., 2011). Siderophores are defined as low-molecular-
98 weight organic compounds (<1kDa) secreted by prokaryotes as part of an Fe-uptake system
99 (Mawji et al., 2008; Vraspir and Butler, 2009). Humic substances (HS) typically come from the
100 degradation of organic matter; they have a strong terrestrial component in the Arctic and are

101 substantially resistant to degradation (Calace et al., 2001; Laglera et al., 2019a; Laglera and van
102 den Berg, 2009). However, marine HS can also be produced *in situ* by bacterial remineralization
103 of biogenic particles (Burkhardt et al., 2014) and grazing (Decho and Gutierrez, 2017; Laglera
104 et al., 2019b). Exopolymeric substances (EPS) are relatively labile macromolecules excreted
105 by microbial cells during all life cycles of phytoplankton growth (Decho and Gutierrez, 2017).
106 During an extreme bloom and following its termination, EPS can dominate from 1% to 50% of
107 the dissolved organic carbon (DOC) pool (Orellana et al., 2003) and together with HS, can be
108 a significant contributor of colloidal organic ligands (Batchelli et al., 2010; Hassler et al., 2011).
109 As microbial exudates, EPS are expected to be produced abundantly up to micromolar levels in
110 surface waters, also at the base of sea ice (Lannuzel et al., 2015), showing the potential to
111 outcompete the stronger ligand group (Hassler et al., 2011). The classification of weak and
112 strong ligand groups based on these three groups is challenging. For example, Slagter et al.
113 (2019) concluded that HS, thought to be a weaker ligand group, can also contain relatively
114 strong ligands ($\log K'_{FeL}$ 11.5 – 12.6), whereas Norman et al. (2015) demonstrated that EPS
115 could have strong binding stability constants as well ($\log K'_{FeL} > 12$).

116 This study focuses on the distribution and chemical properties of natural Fe-binding ligands in
117 Fram Strait and over the northeast Greenland shelf. Concentrations of dissolved and total
118 dissolvable Fe of the same expedition (Krisch et al., submitted) are here combined with the
119 distribution and chemical properties of natural Fe-binding ligands in Fram Strait and over the
120 northeast Greenland shelf (77°N – 81°N and 20°W – 20°E), shedding light on their potential
121 sources and transport and further elucidate the cycling of both Fe and Fe-binding ligands in the
122 rapidly changing Fram Strait region.

123 **Material and methods**

124 **Sampling**

125 Samples were obtained during GEOTRACES expedition GN05 (PS100) on the German
126 research vessel Polarstern during summer 2016. Seawater samples for trace metals and ligands
127 were sampled between 22nd July and 1st September. Details about the cruise track, ice-cover
128 and hydrographic data can be found in the expedition report (Kanzow, 2017).

129 A total of 10 stations were sampled as full depth profiles, 8 - 12 ligand samples per station in
130 Fram Strait and 5 - 7 samples per station over the shelf. Conductivity, temperature, depth
131 (CTD), oxygen and turbidity profiles were obtained using a titanium Seabird SBE 911plus on
132 a trace metal clean rosette frame. The frame was equipped with 24 x 12 L Go-Flo bottles (Ocean

133 Test Equipment) and seawater was collected following the sampling procedures as described
134 by Cutter (2010). Across Fram Strait, samples were collected from 4 different stations (1, 7, 14
135 and 26). Station 1 was located on the eastern side of Fram Strait close to the Svalbard
136 archipelago, while stations 7, 14 and 26 were located towards the western side of Fram Strait
137 (Figure 1). The northeast Greenland shelf section consisted of 6 stations covering the Norske-
138 Westwind trough system, 3 stations were sampled in the Norske Trough (17, 18, and 19) and 1
139 station (11) was sampled in the Westwind Trough (Figure 1). In addition, 2 more stations (21
140 and 22) were sampled in front of the largest glacier of northeast Greenland, the 79N Glacier
141 (Schaffer et al., 2017). Station 21 was located ~20 km away from the glacier front, and station
142 22 was located in front of the floating glacier ice-tongue.

143 Immediately after recovery of the CTD rosette, the Go-Flo bottles were carried into a trace
144 metal clean sampling-container where sub-sampling and filtration was performed under N₂
145 overpressure (~0.2 Bar) using 0.2 µm filters (Acropack 0.8/0.2 µm cartridge filter, Pall). The
146 samples for dissolved Fe analysis were collected in low density polyethylene bottles (LDPE,
147 125 mL, Nalgene) immediately acidified to pH 1.8 using ultraclean HCl (Romil Suprapure) on
148 board as described elsewhere (Krisch et al., submitted).

149 Samples for Fe-binding ligand analysis were collected into acid-cleaned 1000 mL LDPE
150 bottles, immediately stored at -20°C after sampling, and transported to the NIOZ laboratory for
151 analysis. Prior to analysis, samples were thawed in the dark and sub-samples were taken to
152 determine DFe present in the ligand sample bottles for calculation of total Fe-binding ligand
153 concentrations. Therefore approximately 50 mL was collected into 60 mL pre-cleaned LDPE
154 bottles and acidified to pH ~1.8 using concentrated ultrapure hydrochloric acid into final
155 concentration ~0.024 µM (0.2% v/v; Seastar chemicals). The acidified samples were stored at
156 room temperature prior to analysis.

157 **Material handling**

158 Before use, sample bottles were cleaned following three-step cleaning procedure for trace
159 element sample bottles (Cutter, 2010; Middag et al., 2009). All chemicals were prepared using
160 ultrapure water (18.2 MΩ cm, Milli-Q element system, Merck Millipore) and handling
161 performed in an ISO class 7 ultra-clean laboratory with ISO class 5 workspaces. Outside the
162 ultraclean environment, samples were handled in a laminar flood hood (ISO class 5, interflow
163 and AirClean systems).

164 Iron analysis

165 Analysis of DFe was done twice, at GEOMAR, Kiel (Krisch et al., submitted) in samples
166 acidified immediately shipboard, and in subsamples taken from the ligand samples at NIOZ,
167 Texel. In the laboratory at GEOMAR, DFe concentrations were measured by isotope dilution
168 high-resolution inductively coupled plasma-mass spectrometry (HR-ICP-MS, Thermo Fisher
169 Element XR) after pre-concentration (Rapp et al., 2017). The detailed procedure for DFe
170 determination described elsewhere (Krisch et al., submitted).

171 For calculation of $[L_t]$ values, we used the DFe measured from the same bottles as the ligand
172 samples. The DFe samples were pre-concentrated using an automated SeaFAST system (SC-4
173 DX SeaFAST pico; ESI), and analyzed by HR-ICP-MS (Thermo Fisher Element XR) with
174 quantification via standard additions. Accuracy and reproducibility were checked by regular
175 measurements of reference material SAFe D1 (#169) and in-house standards. Results for DFe
176 analyses of reference materials were within the range of May 2013 consensus values (SI Table
177 1). The average overall method blank (SeaFAST & ICP-MS) concentration, determined by
178 measuring acidified ultrapure water as a sample, was 55 ± 7 pM. Dissolved-Fe concentrations
179 measured from the ligand bottles were approximately 15% ($n = 69$) lower than DFe measured
180 from immediately acidified samples as also found by Gerringa et al. (2014)

181 Fe-binding ligands analysis (TAC Method)

182 The CLE-AdCSV technique using 2-(2-thiazolylazo)-p-cresol (TAC, Alfa Aesar) was
183 employed to determine the total Fe-binding ligand concentrations, $[L_t]$ and K'_{FeL} (Croot and
184 Johansson, 2000).

185 A Hanging Mercury Drop Electrode stand (VA663 Metrohm), connected to a PC via an
186 interface (IME663) to control the potentiostat (μ Autolab III, Metrohm Autolab B.V.) was used.
187 The electrodes in the voltammetric stand included a standard Hg drop working electrode, a
188 glassy carbon counter electrode and a double-junction Ag/AgCl reference electrode (3M KCl).
189 For the titration, 10 mL subsample aliquots were distributed into the pre-conditioned Teflon
190 (30 mL Savillex) vials, and buffered to a final pH of 8.05 with MnO_2 -cleaned borate-ammonium
191 (Merck) buffer (final concentration 5 mM). An Fe standard working solution was added to the
192 sample vials, resulting into final concentrations of 0 (twice, no Fe addition); 0.2; 0.4; 0.6; 0.8;
193 1; 1.2; 1.5; 2; 2.5; 3; 4; 6; 8 (twice) nM of Fe. The purpose of double measurement of the no Fe
194 additions was to be absolutely sure this measurement was not influenced by an unconditioned

195 cell. Based on our experience, a small error of the measurement of the highest addition of the
196 titration has large an effect on the result. Therefore, these points were done twice and the ones
197 that gave the best fit were used for the calculation. After Fe additions, TAC was added to each
198 vial at a final concentration of 10 μM . The content in the vials was allowed to equilibrate for at
199 least 8 hours before analysis or typically overnight (Croot and Johansson, 2000). For analysis,
200 the voltammetric scans were in the differential-pulse mode, with a modification from the
201 original procedure (Croot and Johansson, 2000) as previously reported by Slagter et al. (2017).
202 For each sample, two duplicate scans were done at a deposition time of 140s.

203 Fe speciation calculations

204 The data obtained by CLE-AdCSV was interpreted for the ligand parameters, $[\text{L}_t]$ and K'_{FeL} .
205 The data were fitted by a Langmuir model using non-linear regression using the software
206 package R (R Development Core Team, 2011) as described by (Gerringa et al., 2014). A one-
207 ligand model was applied, assuming a single ligand group existed. This model fitted the data
208 well ($\text{SD} < 2\%$; SD of the fitted data from the Langmuir model). The total Fe-binding ligand
209 concentration, $[\text{L}_t]$, is reported in nM equivalents of Fe (nM eq. Fe) and K'_{FeL} values are reported
210 as a common logarithm to base 10 value ($\log K'_{\text{FeL}}$) with respect to inorganic Fe (Fe'). The
211 prime symbol ($'$) is used to denote the fraction not bound by L. For the purpose of this paper,
212 we define $\log K'_{\text{FeL}}$ as the binding strength of ligands.

213 The values of $[\text{L}_t]$ and $\log K'_{\text{FeL}}$ were combined with DFe, measured at GEOMAR to derive
214 concentrations of inorganic Fe, $[\text{Fe}']$. The Fe' species are predominantly Fe-hydroxides, and at
215 a fixed pH of 8.05, $[\text{Fe}']$ can be calculated (Hudson et al., 1992; Liu and Millero, 2002). The
216 calculation of the ligand parameters is described elsewhere (Gerringa et al., 2014; Ružić, 1982;
217 van den Berg, 1982).

218 The center of detection window (D) determines which ligand groups, with respect to their
219 conditional binding strength, can be determined. D is defined as the product of the concentration
220 of TAC and the conditional stability constant of $\text{Fe}(\text{TAC})_2$, $\beta'_{\text{Fe}(\text{TAC})_2}$.

$$221 \quad D_{\text{TAC}} = [\text{TAC}]^2 \times \beta'_{\text{Fe}(\text{TAC})_2}$$

222 The inorganic side reaction coefficient of Fe ($\alpha_{\text{Fe}'}$) of $10^{10.31}$, as determined using Visual
223 MINTEQ software (Gustafsson, 2011), was used to transform the $\beta'_{\text{Fe}(\text{TAC})_2}$ after Croot and
224 Johansson (2000) with respect to Fe^{3+} , into the one with respect to Fe' . Hence, $\beta'_{\text{Fe}(\text{TAC})_2} = 10^{12.1}$

225 was used, resulting in $\log D_{\text{TAC}} = 2.1$. The range of the detection window is assumed to be one
226 order above and below $\log D_{\text{TAC}}$ (Apte et al., 1988).

227 The side reaction coefficient α_{FeL} reflects the ability of ligands to compete for Fe with other
228 ligands and particles. We define α_{FeL} here as the competing strength of ligands, expressed as a
229 logarithmic value, $\log \alpha_{\text{FeL}}$. The saturation state of ligands is indicated by the ratio of $[\text{L}_i]/[\text{DFe}]$.
230 Assuming that other competing metals can be neglected, ligands are undersaturated when
231 $[\text{L}_i]/[\text{DFe}] > 1$, whereas $[\text{L}_i]/[\text{DFe}] \leq 1$ indicate that the ligands are close to saturation (Thuróczy
232 et al., 2010). Statistical analysis of a t-test was performed using the software package R.

233 Results

234 Hydrography

235 The hydrographic features of Fram Strait have been described in detail elsewhere
236 (Beszczynska-Möller et al., 2012; Laukert et al., 2017; Richter et al., 2018; Rudels et al., 2005;
237 Swift and Aagaard, 1981) and are summarized briefly in this study. Water masses were
238 identified using conservative temperature (Θ in $^{\circ}\text{C}$) and absolute salinity (S_A in g/kg) plots
239 following definitions by Tomczak and Godfrey (2003). The data of Θ and S_A were derived from
240 the CTD data using Ocean Data View (Schlitzer, 2018).

241 The relatively warm Atlantic Water (AW) flows northward, carried by the West Spitsbergen
242 Current (WSC) at depths shallower than ~ 500 m at station 1 (Figure 2a). In Fram Strait, about
243 half of AW recirculates back southward, and the other half continues northward into the Arctic
244 Ocean, where it is cooled and freshened, forming Arctic Atlantic Water (AAW) in the process
245 (Bourke et al., 1987; Laukert et al., 2017). The AAW is modified by Pacific-origin water and a
246 large amount of terrestrial runoff in the central Arctic before exiting back through Fram Strait.
247 This modified AAW flows out of the Arctic Ocean along with PSW. These water masses flow
248 southward carried by the East Greenland Current (EGC) (Laukert et al., 2017; Richter et al.,
249 2018; Rudels et al., 2005) in western Fram Strait (at stations 14 and 26; Figure 2a). The western
250 and middle Fram Strait section is substantially affected by the southward flowing Recirculating-
251 Atlantic Water (RAW). The mixing product of RAW (~ 200 to ~ 500 m) and PSW (upper ~ 300
252 m), known as warmer PSW (PSWw) (Rudels et al., 2005; Swift and Aagaard, 1981), was
253 observed in surface waters in between the EGC and WSC at station 7 (Figure 2a). On both sides
254 of Fram Strait, Atlantic Intermediate Water (AIW) (Bourke et al., 1987; Rudels et al., 2005)
255 was present at ~ 500 to ~ 900 m depth, and Norwegian Sea Deep Water (NSDW) (Laukert et al.,
256 2017; Swift and Aagaard, 1981) was present below 1000 m. In this study, AIW and NSDW are
257 categorized as deep waters.

258 Along the northeast Greenland shelf transect, the bathymetry is characterized by the Norske-
259 Westwind Trough system (Figure 1), that features a deep sill in the Norske Trough and a
260 shallow sill in the Westwind Trough (Schaffer et al., 2017). Along this transect, the surface
261 circulation in the C-shaped trough system carried PSW into the Norske-Westwind Trough
262 system in the upper 150-200 m (Bourke et al., 1987; Schaffer et al., 2017). Underneath the PSW
263 layer, modified-AIW (mAIW) was found deeper than ~ 200 -250 m (Figure 2b). For the purpose

264 of this study, mAIW is differentiated as warm-mAIW in the Norske Trough and cold-mAIW in
265 the Westwind Trough based on Schaffer et al. (2017).

266 Dissolved-Fe and Fe-binding ligands

267 Here we present DFe profiles (Figures 3a and 3b) from stations for which Fe-binding ligand
268 samples were also taken. Higher resolution DFe profiles from GEOTRACES expedition GN05
269 are reported by Krisch et al. (submitted).

270 *The Fram Strait transect*

271 DFe concentrations in Fram Strait were in the range of 0.28-1.64 nM. Concentrations of DFe
272 in Fram Strait were low in surface waters (median AW = 0.59 nM, PSW_w = 0.76 nM, PSW =
273 0.48 nM) and increased towards the seafloor to 1.28 nM. On the eastern side, a maximum in
274 DFe was present at ~500 m (1.64 nM). This elevated DFe decreased horizontally westward
275 from station 1 in the east to stations 14 and 26 in the west to concentrations of 0.37 nM (Figure
276 3a).

277 In Fram Strait, [L_t] ranged from 0.79 to 3.00 nM eq. Fe (median AW = 1.20 nM eq. Fe, PSW_w
278 = 1.77 nM eq. Fe, PSW = 1.78 nM eq. Fe, deep waters=1.36 nM eq. Fe; SI Table 2). At stations
279 on the western side (14 and 26), [L_t] was generally higher than at stations in the east and central
280 Fram Strait (1 and 7; Figure 3b). The ratio [L_t]/[DFe] varied between 0.5 and 5.4 (Figure 4a).
281 In the central and eastern regions (stations 1 and 7), the ratio decreased below 250 m, whereas
282 it remained high on the western side of Fram Strait (stations 14 and 26). The ligands were
283 saturated with Fe ([L_t]/[DFe] < 1) at 500 m depth at station 1 and nearly saturated near the sea
284 floor.

285 Whilst [L_t] in surface waters of Fram Strait generally increased from AW (median=1.20 nM eq.
286 Fe) in the east to PSW (median=1.77 nM eq. Fe) in the west (Figures 3b and 5a), the median of
287 [Fe'] in Fram Strait was relatively uniform at 0.05 – 0.15 pM (Figure 5b), apart from the two
288 samples where organic ligands were saturated with Fe.

289 A considerable variation was observed in log K'_{FeL} values (Figure 6a) that ranged from 11.8 to
290 13.9 (median AW = 13.3, PSW_w = 12.9, PSW = 12.4, deep waters = 13.0; Figure 6a). The
291 values of log α_{FeL} (Figure 6b) varied between 1.3 and 4.7 (median AW=4.0, PSW_w=3.7,
292 PSW=3.4, deep waters=3.9; Figure 6b). The highest log α_{FeL} value falls more than 2 orders of
293 magnitude above the log D_{TAC} and thus the highest log K'_{FeL} could not be estimated accurately.

294 Since the ligands were saturated with DFe at 500 m depth at station 1, the calculated α_{FeL} does
295 not represent the actual value of ligand competing strength and thus this data point was not used
296 for calculations.

297 *The northeast Greenland shelf transect*

298 Concentrations of DFe ranged from 0.58 to 1.45 nM in PSW (median DFe = 0.92 nM) and 0.55
299 to 0.78 nM in warm-mAIW (median DFe = 0.68 nM) in the Norske Trough (Figure 3c). Near
300 the 79N Glacier terminus and Westwind Trough, DFe concentrations ranged from 0.71 to 2.10
301 nM (median DFe = 1.16 nM) in PSW and 0.63 to 1.38 nM in cold-mAIW (median DFe = 0.77
302 nM). The highest DFe concentration (2.10 nM) was found in PSW at 30 m depth in front of the
303 glacier terminus (station 22).

304 In the Norske Trough, $[\text{L}_t]$ varied from 1.41 to 3.60 nM eq. Fe in PSW and 0.97 to 2.26 nM eq.
305 Fe in warm-mAIW, whereas near the glacier terminus and Westwind Trough, $[\text{L}_t]$ ranged from
306 1.88 to 2.64 nM eq. Fe in PSW and 2.08 to 2.38 in cold-mAIW (Figure 3d, SI Table 2). On
307 average, $[\text{L}_t]$ was slightly higher at stations near the glacier terminus (stations 21 and 22) than
308 in the Norske Trough, although the highest $[\text{L}_t]$ existed in PSW in the Norske Through (station
309 18) with values up to 3.60 nM eq. Fe at 30 m depth. The ratio of $[\text{L}_t]/[\text{DFe}]$ ranged between 1
310 and 4.4 (Figure 4b), indicating that Fe-binding ligands along the northeast Greenland shelf
311 transect were undersaturated. Near the seafloor at station 19 (Norske Through) and at 50 m
312 depth at station 22 (glacier terminus), nearly saturated ligands were observed.

313 Generally, organic ligands were present at higher concentrations in PSW and mAIW near the
314 glacier terminus and Westwind Trough than in the Norske Trough and Fram Strait (Figure 5a).
315 High concentrations of $[\text{Fe}^*]$ were found in PSW and cold-mAIW in front of the floating glacier
316 ice-tongue (Figure 5b), where the organic ligands were nearly saturated (at station 22; Figure
317 4b). Excluding high $[\text{Fe}^*]$ concentrations in samples where organic ligands were nearly
318 saturated, the median of $[\text{Fe}^*]$ in PSW and mAIW was lower in the Norske Trough (0.16 and
319 0.13 pM) than the Westwind Trough and near the glacier terminus (0.41 and 0.33 pM) (Figure
320 5b).

321 The $\log K'_{\text{FeL}}$ ranged from 12.4–13.2 in the Norske Trough (median PSW=12.7, warm-
322 mAIW=12.9; Figure 6a). Near the glacier terminus and in the Westwind Trough, the $\log K'_{\text{FeL}}$
323 ranged from 12.0 – 12.9 (median PSW and cold-mAIW=12.3, warm-mAIW=12.9; Figure 6a).
324 The $\log K'_{\text{FeL}}$ in the northeast Greenland shelf waters were on average lower than in Fram Strait

325 (Figure 6a). The median values of $\log \alpha_{\text{FeL}}$ in PSW and warm-mAIW in the Norske Trough
326 were 3.9 and 3.7, respectively. In the Westwind Trough and in front of glacier terminus, the
327 median values of $\log \alpha_{\text{FeL}}$ were 3.5 in PSW and 3.4 in cold-mAIW. In general, variation in \log
328 α_{FeL} values over the northeast Greenland shelf was less than in Fram Strait (Figure 6b).

329 Discussion

330 The applied method using TAC was reported to underestimate $[\text{L}_i]$ due to an interaction of TAC
331 with HS binding sites (Laglera et al., 2011; Slagter et al., 2019). However, this method did
332 reveal HS involvement in the ligand pool in different environments (Batchelli et al., 2010;
333 Dulaquais et al., 2018), even in the TPD flow path, where the HS ligands were the dominant
334 group (Slagter et al., 2017). Slagter et al. (2019) compared two CLE-AdCSV techniques, TAC
335 and salicylaldoxime (SA) in the Arctic Ocean and concluded that an offset in $[\text{L}_i]$ between the
336 methods existed. Yet, the increase in $[\text{L}_i]$ due to HS ligands in the TPD was the same for both
337 methods. Thus in our study, we assume that HS is detectable by the TAC method, although $[\text{L}_i]$
338 might be underestimated.

339 Comparison to previous studies

340 Natural ligand measurements have not previously been reported for Fram Strait, but data is
341 available for adjacent areas, notably the Northern Atlantic (Buck et al., 2015; Gerringa et al.,
342 2015; Mohamed et al., 2011) and Arctic Ocean (Slagter et al., 2017; Thuróczy et al., 2011). The
343 studies conducted by Thuróczy et al. (2011), Gerringa et al. (2015) and Slagter et al. (2017)
344 used the same analytical method and data processing technique as in this study, allowing a
345 direct comparison. The here reported $[\text{L}_i]$ in Fram Strait (median PSW = 1.78 nM eq. Fe, PSWw
346 = 1.77 nM eq. Fe, SI Table 2) is comparable to the median $[\text{L}_i]$ (1.61 nM eq. Fe) outside the
347 TPD flow path (Slagter et al., 2017), but slightly higher than $[\text{L}_i]$ reported by Gerringa et al.
348 (2015) for the region between 60 and 33°N in the north west Atlantic Ocean where the median
349 $[\text{L}_i]$ was 1.2 nM eq. Fe (N=8) and reached up to 3.3 nM eq. Fe (SI Figure 2). The median $[\text{L}_i]$
350 in PSW in the western Fram Strait (1.78 nM eq. Fe) and in the northeast Greenland shelf waters
351 (1.96 and 2.17 nM eq. Fe, SI Table 2; surface shelf waters = 2.06 nM eq. Fe; SI Figure 2) was
352 comparable to the median $[\text{L}_i]$ (2.02 nM eq. Fe) reported by Thuróczy et al. (2011) for the Arctic
353 Ocean, but lower than the average $[\text{L}_i]$ (2.79 ± 0.92 , N=19) inside the TPD flow path (Slagter et
354 al., 2017). The elevated $[\text{L}_i]$ in the TPD has been related to HS ligands from fluvial input as
355 well as interaction between sea-ice and sediment (Slagter et al., 2017 and references therein).
356 Gerringa et al. (2015) hypothesized that the Arctic is a source of ligands, largely of humic

357 origin, to the North Atlantic and that $[L_t]$ decreases over time and distance during advection to
358 the south with North Atlantic Deep Water. The current data in Fram Strait indeed confirmed
359 the Arctic can be a source of ligands, likely of humic origin, to regions to the south.

360 We found high $[L_t]$ up to 3.6 nM eq. Fe in the sea-ice covered PSW in the Norske Trough
361 (station 18). Antarctic sea ice is known to be a source of ligands, probably due to EPS excretion
362 at the bottom of the sea ice by diatoms. According to Lannuzel et al. (2015), abundant sea ice
363 diatoms were responsible for relatively high $[L_t]$ in under-ice seawater (4.9 to 9.6 nM eq. Fe;
364 $\log K'_{FeL} \sim 11$ to 13 measured with 1-nitroso-2-naphthol), indicating that EPS could increase $[L_t]$
365 in seawater with sea-ice coverage. As far as we know, no ligand data of Arctic sea ice is
366 available, but the high $[L_t]$ in the sea-ice covered in the Norske Trough, was only slightly lower
367 than the $[L_t]$ reported by Lannuzel et al. (2015) and had comparable relatively high $\log K'_{FeL}$
368 (12.4 - 12.8). As detailed in the introduction, EPS were considered to be part of the weak ligand
369 group (Buck et al., 2016; Bundy et al., 2014; Hassler et al., 2011; Hassler et al., 2017; Laglera
370 and van den Berg, 2009), but Norman et al. (2015) demonstrated that EPS could have strong
371 conditional stability constants ($\log K'_{FeL} > 12$), hence could contribute to the strong ligands
372 detected in surface waters, especially in regions with sea-ice coverage (Krembs et al., 2002;
373 Lannuzel et al., 2015; Lin and Twining, 2012). Thus we suggest that the high $[L_t]$ in sea-ice
374 covered Norske Trough is possibly due to EPS.

375 **Organic ligand sources in Fram Strait**

376 A considerable variation in $\log K'_{FeL}$ values (median AW = 13.3, PSWw = 12.9, PSW = 12.4;
377 Figure 6a), suggests varying contributions of relatively strong and weak ligand groups to the
378 overall ligand pool. The Fe-binding ligands in surface waters of Fram Strait were dominated by
379 a strong ligand group as apparent from the relatively high $\log K'_{FeL} (> 12$; Figure 6a). Despite
380 seasonal NO_3 depletion (Hopwood et al., 2018), this area is productive (Cherkasheva et al.,
381 2014; Smith Jr. et al., 1987). Primary productivity is a known source of organic ligands in
382 surface waters as high ligand concentrations are often associated with high chlorophyll-*a*
383 concentrations (Boye et al., 2001; Gledhill and Buck, 2012; Hunter and Boyd, 2007; Rue and
384 Bruland, 1995; van den Berg, 1995). Besides releasing EPS, marine bacteria (*Alteromonas sp.*)
385 can also synthesize siderophores during a bloom (Hogle et al., 2016). Additionally, following
386 the decline of a phytoplankton bloom, excessive production of EPS can occur (Decho and
387 Gutierrez, 2017). A high weekly average of chlorophyll-*a* concentrations was observed using
388 the MODIS satellite (<https://giovanni.gsfc.nasa.gov/giovanni/>), which indicates the presence of
389 a phytoplankton bloom in June and July. Our sampling time in Fram Strait (end of July to early

390 August, 2016) coincided with the post-bloom period and therefore it seems likely that bloom-
391 associated ligands are responsible for the relatively high concentration of strong ligands in
392 surface waters of Fram Strait.

393 The surface ligand concentration (Figure 5a) on the western side of Fram strait (median
394 PSW=1.78 nM eq. Fe) as well as further into central Fram Strait (median PSWw = 1.77 nM eq.
395 Fe) was somewhat higher than in eastern Fram Strait (median AW = 1.20 nM eq. Fe). Lateral
396 transport of TPD-carried HS ligands from the Arctic (Laglera et al., 2019a; Slagter et al., 2019),
397 likely formed an additional ligand source to surface waters of the western Fram Strait, where
398 PSW flows south with the EGC in the upper ~150 m (Laukert et al., 2017; Richter et al., 2018).
399 This implies both the phytoplankton bloom and TPD may play a role in the surface composition
400 and distribution of ligands in Fram Strait. Atmospheric input does not seem to influence ligand
401 concentrations, Rijkenberg et al. (2008) and Wagener et al. (2008) have shown that there is no
402 input of aeolian Fe-binding ligands during dust deposition events, but dissolution of Fe from
403 the dust does depend on the Fe-binding ligands present in seawater.

404 The organic ligands in Fram Strait were almost saturated near the seafloor (Figure 4a), notably
405 in the region with elevated DFe concentrations (station 7). The western Fram Strait (stations 14
406 and 26) had relatively high, but variably distributed $[L_i]$ over the water column (Figure 3b, SI
407 Figure 1). Slope sediments can serve as a source of ligands to the deeper part of the water
408 column (Buck and Bruland, 2007), however this does not seem to be the case for the station
409 nearest to the slope (station 26), in contrast to the station further into Fram Strait (station 14).
410 Possibly the water transport along the shelf break and interaction with the slope is not constant
411 with time and place. Eddies exist at the shelf break and can reach deep enough to propagate
412 subsurface waters (i.e AIW) toward the inner shelf (Schaffer et al., 2017; Topp and Johnson,
413 1997). In addition, here at this latitude (79°N) the core of the southward flowing RAW mixes
414 with the PSW, and thus substantially contribute to the EGC (Richter et al., 2018). Water
415 transport driven by eddies and RAW intrusion to the EGC may explain the variably distributed
416 $[L_i]$ in the upper (~500m) water column, however, the elevated concentrations in the deeper
417 part of station 14 remain unexplained.

418 [Organic ligand sources over the northeast Greenland shelf](#)

419 In this section, the transect over the northeast Greenland shelf will be discussed in the direction
420 of the general circulation, starting at the southern inlet and going along the Norske Trough
421 towards the 79N Glacier and back towards Fram Strait via the Westwind Trough. The water

422 masses from Fram Strait are propagated toward the inner shelf at the southern inlet (station 17),
423 potentially by eddies, while undergoing pronounced mixing at the shelf edge. Eddy stirring and
424 tidal mixing seem to be persistent features in the Norske Trough inlet (Bourke et al., 1987;
425 Budéus et al., 1997; Schaffer et al., 2017). The balance between release and removal of organic
426 ligands, along with physical water mass mixing (Budéus et al., 1997), is likely responsible for
427 the fairly constant $[L_t]$ observed in the water column at station 17 (Figure 3d).

428 The relatively high concentrations of strong organic ligands (up to 3.60 nM eq. Fe, $\log K'_{FeL}$
429 12.4-12.8) observed in PSW in the Norske Trough were most likely related to an earlier bloom,
430 generating marine HS and EPS ligand groups with relatively strong affinity for Fe. The macro-
431 nutrients (NO_3 , PO_4 , Si; data not shown) at this location were depleted and DFe was low (Figure
432 3d), indicative of a prior bloom. Consistently the chlorophyll-*a* concentration was low at the
433 time of sampling (unpublished data), whereas higher concentrations were observed via satellite
434 in the period prior to sampling (<https://giovanni.gsfc.nasa.gov/giovanni/>). Sato et al. (2007)
435 showed a relation between increasing $[L_t]$ and decreasing chlorophyll-*a* due to zooplankton
436 grazing, and Laglera et al. (2019b) measured an increase in strong organic ligands as a
437 consequence of grazing. This demonstrated that declining blooms can indeed contribute strong
438 organic ligands and increase $[L_t]$ as we observed in our study region. Additionally, black sea-
439 ice with entrapped sediment was spotted during sampling at this location and the melting of
440 black sea-ice can release HS ligands (Genovese et al., 2018) in addition to ligands released from
441 grazing (Decho and Gutierrez, 2017; Laglera et al., 2019b). Also, we cannot eliminate the
442 possible contribution of EPS, either produced *in situ* by sea-ice diatoms (Lannuzel et al., 2015)
443 or released by phytoplankton cells after bloom termination (Decho and Gutierrez, 2017). Recent
444 studies pointed out that HS and EPS can have strong Fe-binding sites (Laglera et al., 2019b;
445 Lannuzel et al., 2015; Norman et al., 2015; Slagter et al., 2019). Therefore, the presence of HS
446 and EPS can contribute to the pool of relatively strong ligands with elevated $[L_t]$ in PSW in the
447 Norske Trough.

448 The ligand-rich PSW in the Norske Trough did not seem to be a significant contributor of
449 organic ligands to either the glacier front or the glacier outflow. Probably ligands produced in
450 the Norske Trough did not yet reach the glacier front. In addition, newly produced ligands
451 associated with primary productivity over the shelf, such as at station 18, are likely to be
452 partially lost due to photodegradation (Barbeau et al., 2001; Powell and Wilson-Finelli, 2003),
453 aggregation and sinking (Cullen et al., 2006) during transport. Either way, a high ligand
454 concentration, such as in the surface waters of Norske Trough, was not observed at the glacier

455 terminus (at stations 21 and 22). At the 79N Glacier terminus, the 80-120 m thick ice-front is
456 limiting direct entry of PSW into the glacier cavity, and at depths of ~80-270 m, water flows
457 eastward away from the glacier front and into the trough system (Schaffer et al., 2017). As
458 warm-mAIW in the Norske Trough has a relatively low $[L_t]$, notably at station 19 on the
459 northern end of the Norske Trough, ligands in the glacier outflow are thus likely produced in
460 the glacier cavity itself. In general, meltwater is relatively poor in DOC compared to coastal
461 seawater, but this DOC may be highly available to bacteria (Paulsen et al., 2017). Hence, the
462 relatively high $[L_t]$ over the entire water column near the 79N Glacier terminus (Figure 3d),
463 could be associated with bacterial remineralization or byproducts of organic matter degradation
464 (Gledhill and Buck, 2012; Gordienko and Laktionov, 1969; Hunter and Boyd, 2007). These
465 ligands would be transported into the Westwind Trough, following the anti-cyclonic water
466 circulation of the Norske-Westwind Trough system (Schaffer et al., 2017; Topp and Johnson,
467 1997). The median of $\log K'_{FeL}$, both in the PSW and mAIW near the glacier terminus (stations
468 21 and 22) and Westwind Trough (station 11) were somewhat lower (Figure 6a) than in the
469 Norske Trough (median $\log K'_{FeL} = 12.3$ versus 12.7 and 12.9). This indicates that different
470 ligand sources shift the characteristics of the overall ligand pool or the ligand pool has
471 undergone physical, chemical or biologically-induced structural alterations during transport,
472 e.g. through photo- or microbial degradation. Although ligands were present at higher
473 concentrations (Figures 3d and 5a), these organic ligands were weaker than in the Norske
474 Trough (Figure 6a). Primary productivity likely dominated the organic ligand sources in the
475 Norske Trough, which may have led to a ligand pool with a relatively high conditional stability
476 constant. In contrast, near the glacier terminus and in Westwind Trough, bacterial
477 remineralization most likely was the dominant ligand source, resulting in more, but overall
478 weaker ligands.

479 Near the glacier terminus and in Westwind Trough, $[Fe']$ was relatively high compared to
480 Norske Trough and Fram Strait (Figure 5b). The glacier acts as a source of Fe and organic-
481 ligand bound Fe, thereby facilitating glacial-Fe transport. However, at the glacier terminus, Fe
482 was prone to precipitation and/or scavenging as $[Fe']$ was enhanced (Figure 5b) and the
483 competing strength of the ligands ($\log \alpha_{FeL}$) was relatively low (Figure 6b). It should be noted
484 here that the complexation of Fe by organic ligands is an equilibrium reaction between
485 complexed Fe and $[Fe']$, where $[Fe']$ is not only determined by competing strength, but also by
486 the scavenging intensity and precipitation reactions. Thus the ligands can effectively release Fe
487 if their competing strength is relatively low and they are outcompeted by scavenging and

488 precipitation processes as shown in the deep Makarov Basin (Slagter et al., 2017; Thuróczy et
489 al., 2011). Availability of $[L_t]$ is thus not a guarantee for complexing (additional) DFe, as it is
490 the overall equilibration between excess ligands, scavenging sites and precipitation that governs
491 the fate of DFe.

492 Biogeochemical provinces of organic ligands

493 This study distinguished three biogeochemical provinces with respect to Fe-binding ligands,
494 based on the influence of different sources of ligands, and hence ligand properties and
495 distribution. The biogeochemical provinces include (1) Fram Strait, (2) Norske Trough and (3)
496 near the glacier terminus and Westwind Trough. The different ligand properties and distribution
497 are reflected in the differences in $[L_t]$ (Figure 5a), $\log K'_{FeL}$ (Figure 6a) and $\log \alpha_{FeL}$ (Figure
498 6b).

499 As described above, in the northward flowing AW of the eastern Fram Strait, strong organic
500 ligands derived from phytoplankton blooms are suggested to dominate the ligand pool. Whereas
501 in the western Fram Strait in southward flowing PSW, part of the ligands probably originated
502 from the Arctic Ocean and partly consists of HS ligands carried by the TPD (Slagter et al.,
503 2017). The average $\log K'_{FeL}$ is significantly higher (SI Table 3) in the AW flow (mean $\log K'_{FeL}$
504 = 13.3 ± 0.3 (1 SD); SI Table 2), compared to the PSW flow in western Fram Strait where the
505 influence of Arctic waters resulted in lower $\log K'_{FeL}$ values (the mean of $\log K'_{FeL}$ 12.4 ± 0.3 (1
506 SD); SI Table 2). The range in $\log K'_{FeL}$ is relatively broad (Figure 6a), implying that different
507 ligand sources supply ligands with various chemical properties, thus different affinity to bind
508 Fe.

509 As detailed, organic ligands were present at higher concentrations near the glacier terminus and
510 Westwind Trough than in the Norske Trough and Fram Strait (Figures 3b and 5a), but the
511 ligands near the glacier terminus and Westwind Trough had a lower affinity for binding Fe
512 (Figure 6a) and a lower competing strength, $\log \alpha_{FeL}$ (Figure 6b). Krisch et al. (submitted)
513 observed that glacial-derived Fe transfer through the Westwind Trough was low because of a
514 net transfer of Fe from the colloidal (thus part of DFe) to the particulate phase with subsequent
515 settling out of the water column, an important removal process in the Fe cycle (Wu et al., 2001).
516 Although organic ligands exist in both the soluble and colloidal fractions (Boye et al., 2010;
517 Fitzsimmons et al., 2015; Thuróczy et al., 2011), part of the colloidal Fe fraction is inert, and
518 not exchangeable (Cullen et al., 2006) and might contribute to coagulation and aggregation and
519 disappearance of Fe. We did not separate soluble and colloidal fractions, but we do demonstrate

520 that the ligands in the glacier outflow and Westwind Trough were relatively weak with a lower
521 competing strength (Figures 6a and 6b). This results in a relatively high $[Fe']$ which in turn
522 allow loss of DFe via precipitation and/or scavenging, consistent with the loss of colloidal Fe
523 observed by Krisch et al. (submitted).

524 Global warming causes rapid environmental changes in the Arctic and sub-Arctic Oceans
525 (Gascard et al., 2008; IPCC, 2014) to which Fram Strait belong (Ekwurzel et al., 2001; Schuur
526 et al., 2015). These changes may alter the properties and distribution of organic Fe-binding
527 ligands. Melting of sea-ice influences biological activity (Arrigo et al., 2008; Meier et al., 2014)
528 and without considering possible nutrient depletion, this may increase the release of strong
529 organic ligands. An increased competing strength of organic ligands enhances the ability of
530 ligands to stabilize additional Fe input, potentially increasing the DFe export from Greenland
531 towards the open ocean if the timing and location of DFe input coincides with the presence of
532 these ligands. Not much is known about Fe limitation in the Nordic Seas, although potential Fe
533 limitation was reported for the Nansen Basin of the Arctic Ocean (Rijkenberg et al., 2018). Also
534 the Iceland Basin in the North Atlantic experiences seasonal Fe limitation (Hopwood et al.,
535 2018; Mohamed et al., 2011; Nielsdóttir et al., 2009; Ryan-Keogh et al., 2013). Enhanced
536 transport of ligand bound Fe from the Arctic may thus have a profound effect on primary
537 productivity in the high-latitude North Atlantic. However, such changes must also be
538 considered alongside other physical/chemical perturbations in the region as a result of ongoing
539 changes such as the increase in freshwater discharge around Greenland. The complex interplay
540 between Fe and ligand sources versus scavenging and coagulation will need to be better
541 constrained to enable accurate predictions of changes in the biogeochemical cycle of Fe in the
542 globally important northern high latitudes, as well as elsewhere.

543 **Conclusion**

544 This study provides a connection between the previous reports on organic Fe-binding ligands
545 in the Arctic Ocean and North Atlantic Ocean, as well as insight into the competing strength of
546 organic Fe-binding ligands that regulate DFe transport from a Greenland glacier. Our results
547 indicate that the Fe-binding ligands in surface waters of Fram Strait originate from microbial
548 activity with addition from southward-flowing TPD transported terrestrial ligands on the
549 western side of Fram Strait. Given that the $[L_i]$ in western Fram Strait is intermediate to the
550 higher concentrations reported for the Arctic and the lower concentrations reported for the
551 North Atlantic, this confirms the decreasing $[L_i]$ southward from the Arctic Ocean.

552 In the Norske Trough, the remnant from an earlier bloom was likely the main source of organic
553 Fe-binding ligands in surface waters, as the contribution of ligands can be substantial at the
554 base of sea-ice. The elevated $[L_i]$ at stations near the 79N Glacier terminus is probably
555 associated with remineralization of glacially-derived organic matter. Our data shows that even
556 though significantly higher concentrations of organic ligands were present at the vicinity of
557 79N Glacier terminus and in the Westwind Trough (outflow) than in the Norske Trough
558 (inflow), the organic ligands are weaker and therefore can compete less efficiently with
559 scavenging processes and precipitation. Especially close to the glacier, ligands have a weaker
560 affinity for binding Fe. We show that transport of Fe in the glacial outflow is potentially
561 regulated by ligands as has been anticipated from comparisons of particulate and dissolved Fe
562 distributions in several systems worldwide. Additionally, our results reveal the underlying
563 mechanism where the lower ligand binding strength and consequently higher $[Fe^*]$ (rather than
564 a low concentration of ligands) result in more precipitation of Fe-oxyhydroxides or/and
565 scavenging. Thereby only a small part of the glacial DFe will be transported over the shelf into
566 the ocean. Different sources supply ligands with various chemical properties, resulting in
567 distinctive properties of the ligand pool among regions.

568 Rapid environmental changes due to global warming will cause increased river runoff and
569 glacial melt into the Arctic Ocean, increasing gross Fe supply into the Arctic basin. However,
570 it is the combination of availability and binding strength of organic ligands that regulate DFe
571 transport and distribution in Fram Strait region. Thus, to understand the consequences of global
572 warming in the Arctic and sub-Arctic Oceans for the biogeochemical cycle of Fe, the changes
573 in the biogeochemical cycle of the ligands need to be understood as well. Especially glacial
574 systems will need to be investigated further to determine if there is strong temporal variability

575 in the concentration and competing strength of Fe-binding ligands or if large differences exist
576 between different glaciers.

577 **Figure captions**

- 578 • Figure 1. Map of the study area with schematic currents. The yellow marks indicate the
579 station positions in this study sampled by a trace metal clean CTD Rosette sampling
580 system. The blue dots indicate the stations sampled by a large CTD sampling system.
581 The Fram Strait transect consists of stations 1, 7, 14 and 26. The northeast Greenland
582 shelf transect consist of stations 17, 18 and 19 in the Norske Trough, stations 21 and
583 22 near the 79N Glacier terminus, and station 11 in the Westwind Trough. The West-
584 Spitsbergen Current (WSC, indicated by red arrows) brings warm Atlantic Water (AW)
585 into the Arctic Ocean. The southward flowing East Greenland (EGC, grey arrows)
586 carries part of the recirculated WSC as well as outflow Polar Surface Water (PSW)
587 from the Arctic Ocean. The yellow arrows indicate the anti-cyclonic circulation
588 through the trough system. This figure is adapted from Schaffer et al., (2017) and based
589 on Bourke et al., (1987).
- 590 • Figure 2. The distribution of absolute salinity (S_A), conservative temperature (Θ) and
591 potential density (σ_θ) along the transects with the various water masses indicated. (a):
592 Absolute salinity with potential density as contours in the Fram Strait transect; (b):
593 conservative temperature with potential density as contours along the northeast
594 Greenland shelf transect. The square symbol indicates the station (22) in front of the
595 glacier terminus, and the dot symbol indicates the station (21) at ~20 km distance from
596 the glacier terminus.
- 597 • Figure 3. The distribution of dissolved Fe (DFe, data from Krisch et al., submitted) and
598 total Fe-binding ligand concentrations ($[L_t]$) of both transects; the Fram Strait transect
599 on the left and the northeast Greenland shelf transect on the right. DFe concentrations
600 (a,c) and $[L_t]$ (b,d). Along the northeast Greenland shelf transect, the square symbol
601 indicates the station in front of the glacier terminus, and the dot symbol indicates the
602 station at ~20 km distance from the glacier terminus.
- 603 • Figure 4. The distribution of ligand saturation ($[L_t]/DFe$) of both transects; the Fram
604 Strait transect (a) and the northeast Greenland shelf transect (b). Along the northeast
605 Greenland shelf transect, the square symbol indicates the station in front of the glacier
606 terminus, and the dot symbol indicates the station at ~20 km distance from the glacier
607 terminus.
- 608 • Figure 5. Boxplots of the concentrations of (a) total organic Fe-binding ligands, $[L_t]$,
609 and (b) inorganic iron, $[Fe^*]$, from all stations in Fram Strait and over the northeast
610 Greenland shelf (the Norske Trough and Westwind Trough), categorized by water
611 mass. Indicated are the median value by a thick horizontal line, the box contains the
612 first and third quartiles, the whiskers are the range of data excluding the outliers. The
613 circles indicate the outliers being 1.5* interquartile range from the box (Teetor, 2011).
- 614 • Figure 6. Boxplots of the conditional stability constants (binding strength), $\log K'_{FeL}$ (a)
615 and side reaction coefficients (competing strength), $\log \alpha_{FeL}$ (b) from all stations in
616 Fram Strait and over the northeast Greenland shelf (the Norske Trough and Westwind
617 Trough), categorized by water mass. The detail explanation of the boxplot is as
618 described in Figure 5.

Supplementary Information (SI):

- SI Figure 1. The depth profiles of dissolved-Fe (DFe) and total ligand concentrations [L_t] for each station in Fram Strait and over the northeast Greenland shelf. Station numbers are indicated at the bottom right of each figure. Figures are made using the software package R.
- SI Figure 2. Boxplots of the total Fe-binding ligand concentrations, [L_t], from existing studies in the Arctic Ocean (Slagter et al., 2017; Thuróczy et al., 2011) and the North Atlantic Ocean (Gerringa et al., 2014). The letter “S” refers to surface data. Surface samples from Slagter et al., (2017) were selected from Polar Surface Water (PSW) at stations inside (81, 87, 91, 96) and outside (50, 64 and 69) the Transpolar Drift (TPD), based on the TPD definition as described in the original paper of Slagter et al., (2017). Surface samples from Thuróczy et al, (2011) were taken from upper 200m at stations in Makarov and Amundsen Basin. Surface samples from Gerringa et al., (2014) were taken from upper 200m at stations 2 and 5 in the North Atlantic Ocean.
- SI Table 1. Values for dissolved-Fe analyses of reference materials. The consensus values were obtained from <http://www.geotraces.org/>
- SI Table 2. The summary of ligand data grouped by water mass.
- SI Table 3. T-test statistics summary. The significance levels are $p < 0.005^{***}$, $p < 0.01^{**}$, $p < 0.05^*$ and $p < 0.1$

Acknowledgements

Authors would like to thank Captain Schwarze and his crew of the RV Polarstern, as well as chief scientist Torsten Kanzow, for their effort and support during sample collection. Patrick Laan is acknowledged for analyzing DFe for Fe-binding ligands calculation. We thank anonymous reviewers for their comments that improved the manuscript considerably. IA was financed by Indonesia Endowment Fund for Education (LPDP), and SK was financed by GEOMAR and the German Research Foundation (DFG award number AC 217/1-1 to E. P. A). Figures 1 to 4 are made using the software Ocean Data View 5.1.7 (Schlitzer, 2018). Figures 5 and 6 are made using the software package R version 3.4.2. Data can be accessed online at <https://doi.org/10.25850/nioz/7b.b.u.>

References

- Abualhaija, M.M. and van den Berg, C.M.G., 2014. Chemical speciation of iron in seawater using catalytic cathodic stripping voltammetry with ligand competition against salicylaldehyde. *Marine Chemistry*, 164: 60-74.
- Apte, S.C., Gardner, M.J. and Ravenscroft, J.E., 1988. An evaluation of voltammetric titration procedures for the determination of trace metal complexation in natural waters by use of computers simulation. *Analytica Chimica Acta*, 212: 1-21.
- Arrigo, K.R., van Dijken, G. and Pabi, S., 2008. Impact of a shrinking Arctic ice cover on marine primary production. *Geophysical Research Letters*, 35(19).
- Barbeau, K., Rue, E.L., Bruland, K.W. and Butler, A., 2001. Photochemical cycling of iron in the surface ocean mediated by microbial iron(III)-binding ligands. *Nature*, 413(6854): 409-413.
- Batchelli, S., Muller, F.L.L., Chang, K.-C. and Lee, C.-L., 2010. Evidence for Strong but Dynamic Iron–Humic Colloidal Associations in Humic-Rich Coastal Waters. *Environmental Science & Technology*, 44(22): 8485-8490.
- Beszczyńska-Möller, A., Fahrback, E., Schauer, U. and Hansen, E., 2012. Variability in Atlantic water temperature and transport at the entrance to the Arctic Ocean, 1997–2010. *ICES Journal of Marine Science*, 69(5): 852-863.
- Bourke, R.H., Newton, J.L., Paquette, R.G. and Tunnicliffe, M.D., 1987. Circulation and water masses of the East Greenland shelf. *Journal of Geophysical Research: Oceans*, 92(C7): 6729-6740.
- Boyd, P.W. et al., 2000. A mesoscale phytoplankton bloom in the polar Southern Ocean stimulated by iron fertilization. *Nature*, 407: 695.
- Boye, M. et al., 2010. Significant portion of dissolved organic Fe complexes in fact is Fe colloids. *Marine Chemistry*, 122(1): 20-27.
- Boye, M. et al., 2001. Organic complexation of iron in the Southern Ocean. *Deep-Sea Research Part I: Oceanographic Research Papers*, 48(6): 1477-1497.
- Buck, K.N. and Bruland, K.W., 2007. The physicochemical speciation of dissolved iron in the Bering Sea, Alaska. *Limnology and Oceanography*, 52(5): 1800-1808.
- Buck, K.N., Gerringa, L.J.A. and Rijkenberg, M.J.A., 2016. An Intercomparison of Dissolved Iron Speciation at the Bermuda Atlantic Time-series Study (BATS) Site: Results from GEOTRACES Crossover Station A. *Frontiers in Marine Science*, 3(262).
- Buck, K.N., Sohst, B. and Sedwick, P.N., 2015. The organic complexation of dissolved iron along the U.S. GEOTRACES (GA03) North Atlantic Section. *Deep Sea Research Part II: Topical Studies in Oceanography*, 116: 152-165.
- Budéus, G., Schneider, W. and Kattner, G., 1997. Distribution and exchange of water masses in the Northeast Water polynya (Greenland Sea). *Journal of Marine Systems*, 10(1): 123-138.
- Bundy, R.M., Biller, D.V., Buck, K.N., Bruland, K.W. and Barbeau, K.A., 2014. Distinct pools of dissolved iron-binding ligands in the surface and benthic boundary layer of the California Current. *Limnology and Oceanography*, 59(3): 769-787.
- Burkhardt, B.G., Watkins-Brandt, K.S., Defforey, D., Paytan, A. and White, A.E., 2014. Remineralization of phytoplankton-derived organic matter by natural populations of heterotrophic bacteria. *Marine Chemistry*, 163: 1-9.
- Calace, N. et al., 2001. Aquatic humic substances in pack ice-seawater-sediment system. *International Journal of Environmental Analytical Chemistry*, 79(4): 315-329.
- Cherkasheva, A. et al., 2014. Influence of the physical environment on polar phytoplankton blooms: A case study in the Fram Strait. *Journal of Marine Systems*, 132: 196-207.
- Croot, P.L. and Johansson, M., 2000. Determination of Iron Speciation by Cathodic Stripping Voltammetry in Seawater Using the Competing Ligand 2-(2-Thiazolylazo)-p-cresol (TAC). *Electroanalysis*, 12(8): 565-576.
- Cullen, J.T., Bergquist, B.A. and Moffett, J.W., 2006. Thermodynamic characterization of the partitioning of iron between soluble and colloidal species in the Atlantic Ocean. *Marine Chemistry*, 98(2): 295-303.

- Cutter, G., Andersson, P., Codispoti, L., Croot, P. François, R., Lohan, M. C., Obata, H. and Rutgers v. d. Loeff, M., 2010. Sampling and Sample-handling Protocols for GEOTRACES Cruises.
- De Baar, H.J.W., 1990. On iron limitation of the Southern Ocean : experimental observations in the Weddell and Scotia Seas. *Marine Ecol. Prog. Ser.*, 65: 105-122.
- Decho, A.W. and Gutierrez, T., 2017. Microbial Extracellular Polymeric Substances (EPSs) in Ocean Systems. *Frontiers in Microbiology*, 8(922).
- Dulaquais, G. et al., 2018. The biogeochemistry of electroactive humic substances and its connection to iron chemistry in the North East Atlantic and the Western Mediterranean Sea. *Journal of Geophysical Research: Oceans*, 123(8): 5481-5499.
- Ekwurzel, B., Schlosser, P., Mortlock, R.A., Fairbanks, R.G. and Swift, J.H., 2001. River runoff, sea ice meltwater, and Pacific water distribution and mean residence times in the Arctic Ocean. *Journal of Geophysical Research: Oceans*, 106(C5): 9075-9092.
- Fitzsimmons, J. N., et al. (2015). "The composition of dissolved iron in the dusty surface ocean: An exploration using size-fractionated iron-binding ligands." *Marine Chemistry* 173: 125-135.
- Gascard, J.-C. et al., 2008. Exploring Arctic Transpolar Drift During Dramatic Sea Ice Retreat. *Eos, Transactions American Geophysical Union*, 89(3): 21-22.
- Gerringa, L.J., Rijkenberg, M.J., Thuróczy, C.-E. and Maas, L.R., 2014. A critical look at the calculation of the binding characteristics and concentration of iron complexing ligands in seawater with suggested improvements. *Environmental Chemistry*, 11(2): 114-136.
- Gerringa, L.J.A., Rijkenberg, M.J.A., Schoemann, V., Laan, P. and de Baar, H.J.W., 2015. Organic complexation of iron in the West Atlantic Ocean. *Marine Chemistry*, 177: 434-446.
- Gledhill, M. and Buck, K., 2012. The organic complexation of iron in the marine environment: A review. *Frontiers in Microbiology*, 3(69).
- Gledhill, M. and van den Berg, C.M.G., 1994. Determination of complexation of iron(III) with natural organic complexing ligands in seawater using cathodic stripping voltammetry. *Marine Chemistry*, 47(1): 41-54.
- Gordienko, P.A. and Laktionov, A.F., 1969. Section 3.3 - Circulation and physics of the Arctic basin waters. In: A.L. Gordon and F.W.G. Baker (Editors), *Oceanography*. Pergamon, pp. 94-112.
- Hassler, C.S., Alasonati, E., Mancuso Nichols, C.A. and Slaveykova, V.I., 2011. Exopolysaccharides produced by bacteria isolated from the pelagic Southern Ocean — Role in Fe binding, chemical reactivity, and bioavailability. *Marine Chemistry*, 123(1-4): 88-98.
- Hassler, C.S., van den Berg, C.M.G. and Boyd, P.W., 2017. Toward a Regional Classification to Provide a More Inclusive Examination of the Ocean Biogeochemistry of Iron-Binding Ligands. *Frontiers in Marine Science*, 4(19).
- Hogle, S.L., Bundy, R.M., Blanton, J.M., Allen, E.E. and Barbeau, K.A., 2016. Copiotrophic marine bacteria are associated with strong iron-binding ligand production during phytoplankton blooms. *Limnology and Oceanography Letters*, 1(1): 36-43.
- Hopwood, M.J. et al., 2018. Non-linear response of summertime marine productivity to increased meltwater discharge around Greenland. *Nature Communications*, 9(1): 3256.
- Hudson, R.J.M., Covault, D.T. and Morel, F.M.M., 1992. Investigations of iron coordination and redox reactions in seawater using ⁵⁹Fe radiometry and ion-pair solvent extraction of amphiphilic iron complexes. *Marine Chemistry*, 38(3): 209-235.
- Hunter, K.A. and Boyd, P.W., 2007. Iron-binding ligands and their role in the ocean biogeochemistry of iron. 4(4): 221-232.
- IPCC, 2014. *Climate Change 2014: Synthesis Report. Contribution of Working Groups I, II and III to the Fifth Assessment Report of the Intergovernmental Panel on Climate Change* [Core Writing Team, R.K. Pachauri and L.A. Meyer (eds.)]. (IPCC, Geneva, Switzerland.): 151 pp.
- Kanzow, T., 2017. The Expedition PS100 of the Research Vessel POLARSTERN to the Fram Strait in 2016. 1866-3192.
- Klunder, M.B. et al., 2012. Dissolved iron in the Arctic shelf seas and surface waters of the central Arctic Ocean: Impact of Arctic river water and ice-melt. *Journal of Geophysical Research: Oceans*, 117(C1).
- Krembs, C., Eicken, H., Junge, K. and Deming, J.W., 2002. High concentrations of exopolymeric substances in Arctic winter sea ice: implications for the polar ocean carbon cycle and

- cryoprotection of diatoms. *Deep Sea Research Part I: Oceanographic Research Papers*, 49(12): 2163-2181.
- Kuma, K., Nishioka, J. and Matsunaga, K., 1996. Controls on iron(III) hydroxide solubility in seawater: The influence of pH and natural organic chelators. *Limnology and Oceanography*, 41(3): 396-407.
- Laglera, L.M., Battaglia, G. and van den Berg, C.M.G., 2011. Effect of humic substances on the iron speciation in natural waters by CLE/CSV. *Marine Chemistry*, 127(1): 134-143.
- Laglera, L.M. et al., 2019a. First Quantification of the Controlling Role of Humic Substances in the Transport of Iron Across the Surface of the Arctic Ocean. *Environmental science & technology*.
- Laglera, L.M. et al., 2019b. Iron organic speciation during the LOHAFEX experiment: Iron ligands release under biomass control by copepod grazing. *Journal of Marine Systems*: 103151.
- Laglera, L.M. and van den Berg, C.M.G., 2009. Evidence for geochemical control of iron by humic substances in seawater. *Limnology and Oceanography*, 54(2): 610-619.
- Lannuzel, D., Grotti, M., Abelmoschi, M.L. and van der Merwe, P., 2015. Organic ligands control the concentrations of dissolved iron in Antarctic sea ice. *Marine Chemistry*, 174: 120-130.
- Laukert, G. et al., 2017. Ocean circulation and freshwater pathways in the Arctic Mediterranean based on a combined Nd isotope, REE and oxygen isotope section across Fram Strait. *Geochimica et Cosmochimica Acta*, 202: 285-309.
- Lin, H. and Twining, B.S., 2012. Chemical speciation of iron in Antarctic waters surrounding free-drifting icebergs. *Marine Chemistry*, 128-129: 81-91.
- Liu, X. and Millero, F.J., 2002. The solubility of iron in seawater. *Marine Chemistry*, 77(1): 43-54.
- Martin, J.H. and Fitzwater, S.E., 1988. Iron deficiency limits phytoplankton growth in the north-east Pacific subarctic. *Nature*, 331(6154): 341-343.
- Mawji, E. et al., 2008. Hydroxamate Siderophores: Occurrence and Importance in the Atlantic Ocean. *Environmental Science & Technology*, 42(23): 8675-8680.
- Measures, C.I., 1999. The role of entrained sediments in sea ice in the distribution of aluminium and iron in the surface waters of the Arctic Ocean. *Marine Chemistry*, 68(1): 59-70.
- Meier, W.N. et al., 2014. Arctic sea ice in transformation: A review of recent observed changes and impacts on biology and human activity. *Reviews of Geophysics*, 52(3): 185-217.
- Middag, R., De Baar, H., Laan, P. and Bakker, K., 2009. Dissolved aluminium and the silicon cycle in the Arctic Ocean. *Marine Chemistry*, 115(3-4): 176-195.
- Millero, F.J., Huang, F. and Laferiere, A.L., 2002. The solubility of oxygen in the major sea salts and their mixtures at 25°C. *Geochimica et Cosmochimica Acta*, 66(13): 2349-2359.
- Mohamed, K.N., Steigenberger, S., Nielsdottir, M.C., Gledhill, M. and Achterberg, E.P., 2011. Dissolved iron(III) speciation in the high latitude North Atlantic Ocean. *Deep Sea Research Part I: Oceanographic Research Papers*, 58(11): 1049-1059.
- Nielsdóttir, M.C., Moore, C.M., Sanders, R., Hinz, D.J. and Achterberg, E.P., 2009. Iron limitation of the postbloom phytoplankton communities in the Iceland Basin. *Global Biogeochemical Cycles*, 23(3).
- Norman, L. et al., 2015. The role of bacterial and algal exopolymeric substances in iron chemistry. *Marine Chemistry*, 173: 148-161.
- Orellana, M.V. et al., 2003. Tracing the source and fate of biopolymers in seawater: application of an immunological technique. *Marine chemistry*, 83(1-2): 89-99.
- Paulsen, M.L. et al., 2017. Carbon Bioavailability in a High Arctic Fjord Influenced by Glacial Meltwater, NE Greenland. *Frontiers in Marine Science*, 4(176).
- Powell, R.T. and Wilson-Finelli, A., 2003. Photochemical degradation of organic iron complexing ligands in seawater. *Aquatic Sciences*, 65(4): 367-374.
- R Development Core Team, R., 2011. R: A language and environment for statistical computing. R foundation for statistical computing, Vienna, Austria.
- Rapp, I., Schlosser, C., Rusiecka, D., Gledhill, M. and Achterberg, E.P., 2017. Automated preconcentration of Fe, Zn, Cu, Ni, Cd, Pb, Co, and Mn in seawater with analysis using high-resolution sector field inductively-coupled plasma mass spectrometry. *Analytica Chimica Acta*, 976: 1-13.

- Richter, M.E., von Appen, W.J. and Wekerle, C., 2018. Does the East Greenland Current exist in the northern Fram Strait? *Ocean Sci.*, 14(5): 1147-1165.
- Rijkenberg, M.J.A. et al., 2008. Changes in iron speciation following a Saharan dust event in the tropical North Atlantic Ocean. *Marine Chemistry*, 110(1): 56-67.
- Rijkenberg, M.J.A., Slagter, H.A., Rutgers van der Loeff, M., van Ooijen, J. and Gerringa, L.J.A., 2018. Dissolved Fe in the Deep and Upper Arctic Ocean With a Focus on Fe Limitation in the Nansen Basin. 5(88).
- Rudels, B. et al., 2005. The interaction between waters from the Arctic Ocean and the Nordic Seas north of Fram Strait and along the East Greenland Current: results from the Arctic Ocean-02 Oden expedition. *Journal of Marine Systems*, 55(1): 1-30.
- Rudels, B. et al., 2015. Circulation and transformation of Atlantic water in the Eurasian Basin and the contribution of the Fram Strait inflow branch to the Arctic Ocean heat budget. *Progress in Oceanography*, 132: 128-152.
- Rue, E.L. and Bruland, K.W., 1995. Complexation of iron(III) by natural organic ligands in the Central North Pacific as determined by a new competitive ligand equilibration/adsorptive cathodic stripping voltammetric method. *Marine Chemistry*, 50(1): 117-138.
- Ružić, I., 1982. Theoretical aspects of the direct titration of natural waters and its information yield for trace metal speciation. *Analytica Chimica Acta*, 140(1): 99-113.
- Ryan-Keogh, T.J. et al., 2013. Spatial and temporal development of phytoplankton iron stress in relation to bloom dynamics in the high-latitude North Atlantic Ocean. *Limnology and Oceanography*, 58(2): 533-545.
- Schaffer, J. et al., 2017. Warm water pathways toward Nioghalvfjærdsfjorden Glacier, Northeast Greenland. *Journal of Geophysical Research: Oceans*, 122(5): 4004-4020.
- Schlitzer, R., 2018. Ocean Data View.
- Schuur, E.A.G. et al., 2015. Climate change and the permafrost carbon feedback. *Nature*, 520: 171.
- Slagter, H.A., Laglera, L.M., Sukekava, C. and Gerringa, L.J.A., 2019. Fe-binding Organic Ligands in the Humic-Rich TransPolar Drift in the Surface Arctic Ocean using Multiple Voltammetric Methods. *Journal of Geophysical Research: Oceans*, 124(3): 1491-1508.
- Slagter, H.A. et al., 2017. Organic Fe speciation in the Eurasian Basins of the Arctic Ocean and its relation to terrestrial DOM. *Marine Chemistry*, 197: 11-25.
- Smith Jr., W.O., Baumann, M.E.M., Wilson, D.L. and Aletsee, L., 1987. Phytoplankton biomass and productivity in the marginal ice zone of the Fram Strait during summer 1984. 92(C7): 6777-6786.
- Swift, J.H. and Aagaard, K., 1981. Seasonal transitions and water mass formation in the Iceland and Greenland seas. *Deep Sea Research Part A. Oceanographic Research Papers*, 28(10): 1107-1129.
- Thuróczy, C.-E. et al., 2011. Distinct trends in the speciation of iron between the shallow shelf seas and the deep basins of the Arctic Ocean. 116(C10).
- Thuróczy, C.E. et al., 2010. Speciation of Fe in the Eastern North Atlantic Ocean. *Deep Sea Research Part I: Oceanographic Research Papers*, 57(11): 1444-1453.
- Tomczak, M. and Godfrey, J., 2003. *Regional oceanography: An introduction*, 390 pp. Daya, New Delhi.
- Topp, R. and Johnson, M., 1997. Winter intensification and water mass evolution from yearlong current meters in the Northeast Water Polynya. *Journal of Marine Systems*, 10(1): 157-173.
- van den Berg, C.M.G., 1982. Determination of copper complexation with natural organic ligands in seawater by equilibration with MnO₂ I. Theory. *Marine Chemistry*, 11(4): 307-322.
- van den Berg, C.M.G., 1995. Evidence for organic complexation of iron in seawater. *Marine Chemistry*, 50(1): 139-157.
- van den Berg, C.M.G., 2006. Chemical speciation of iron in seawater by cathodic stripping voltammetry with dihydroxynaphthalene. *Analytical Chemistry*, 78(1): 156-163.
- Velasquez, I.B. et al., 2016. Ferrioxamine siderophores detected amongst iron binding ligands produced during the remineralization of marine particles. *Frontiers in Marine Science*, 3: 172.
- Vraspir, J.M. and Butler, A., 2009. Chemistry of marine ligands and siderophores. *Annual Review of Marine Science*, 1: 43-63.

- Wagener, T., Pulido-Villena, E. and Guieu, C., 2008. Dust iron dissolution in seawater: Results from a one-year time-series in the Mediterranean Sea. *Geophysical Research Letters*, 35(16).
- Wu, J., Boyle, E., Sunda, W. and Wen, L.-S., 2001. Soluble and Colloidal Iron in the Oligotrophic North Atlantic and North Pacific. *Science*, 293(5531): 847-849.

Fig.1

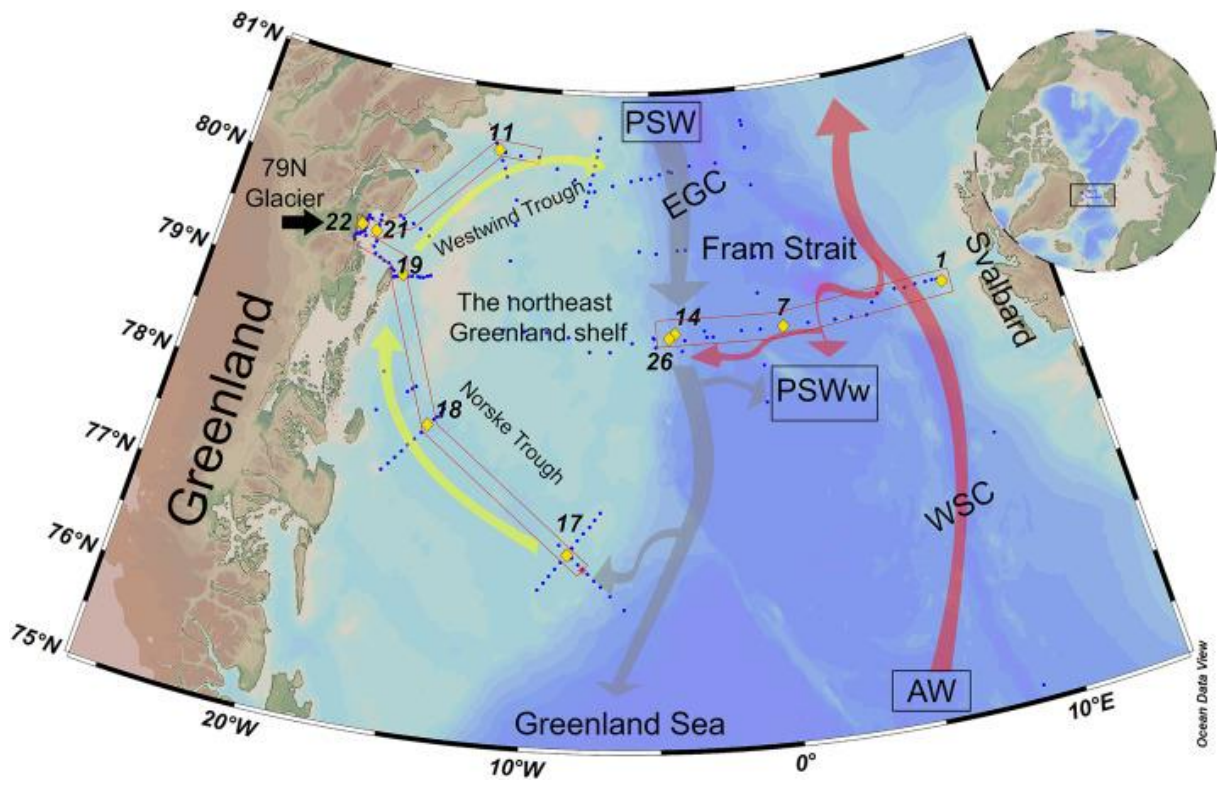


Fig. 2

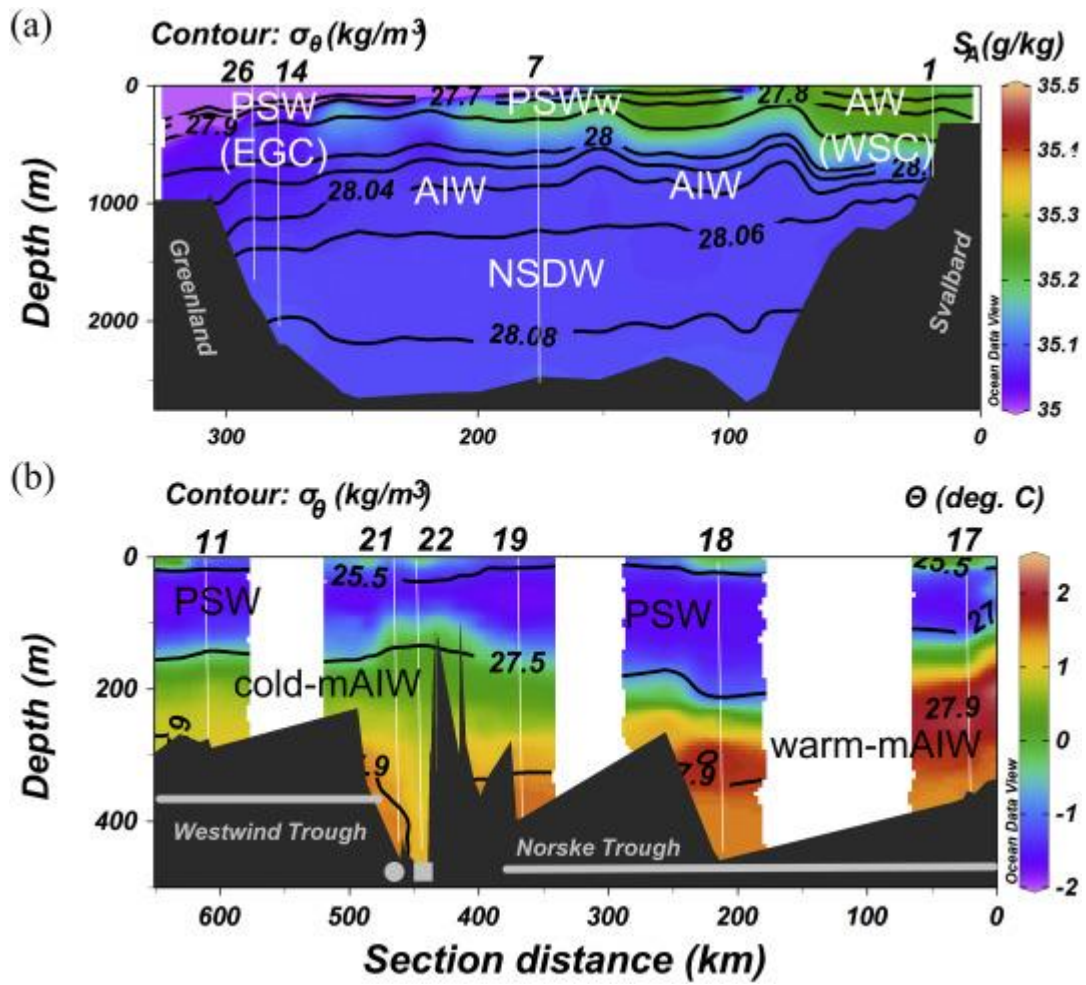


Fig. 3

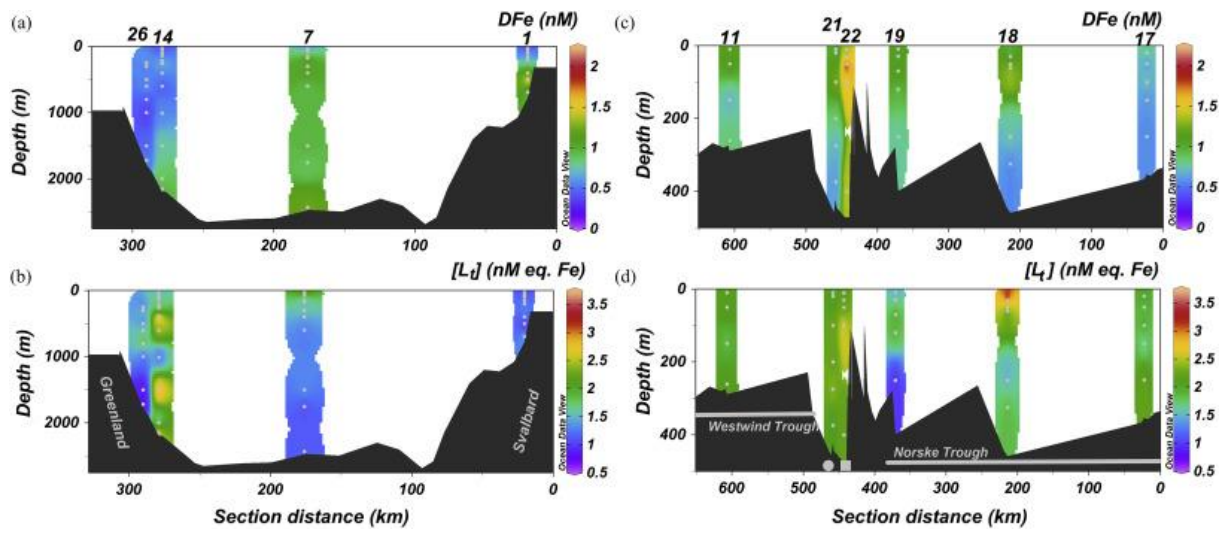


Fig. 4

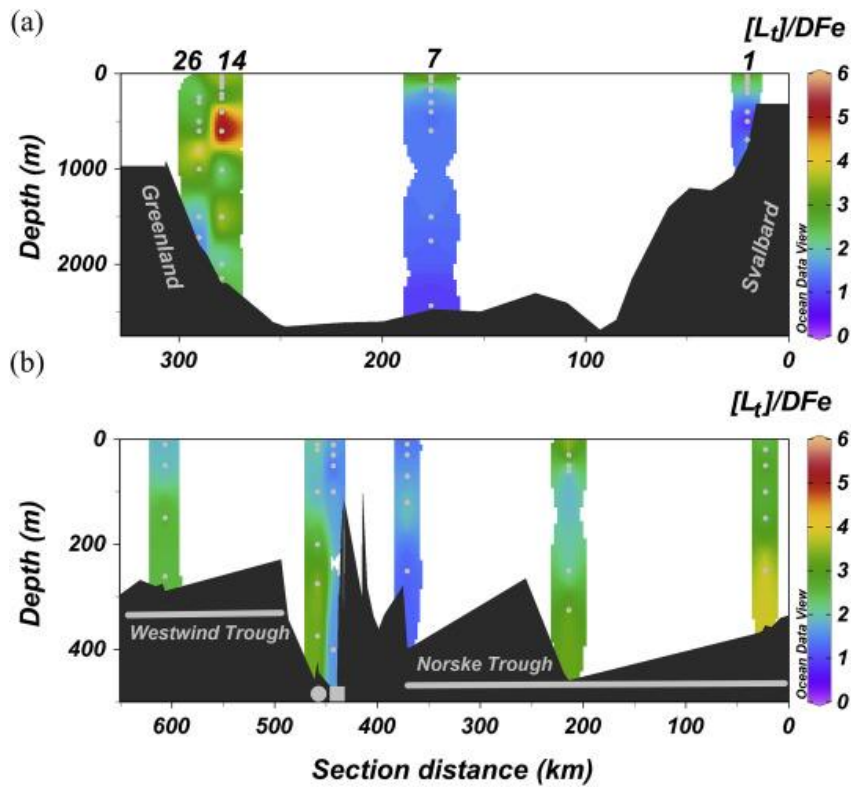


Fig. 5

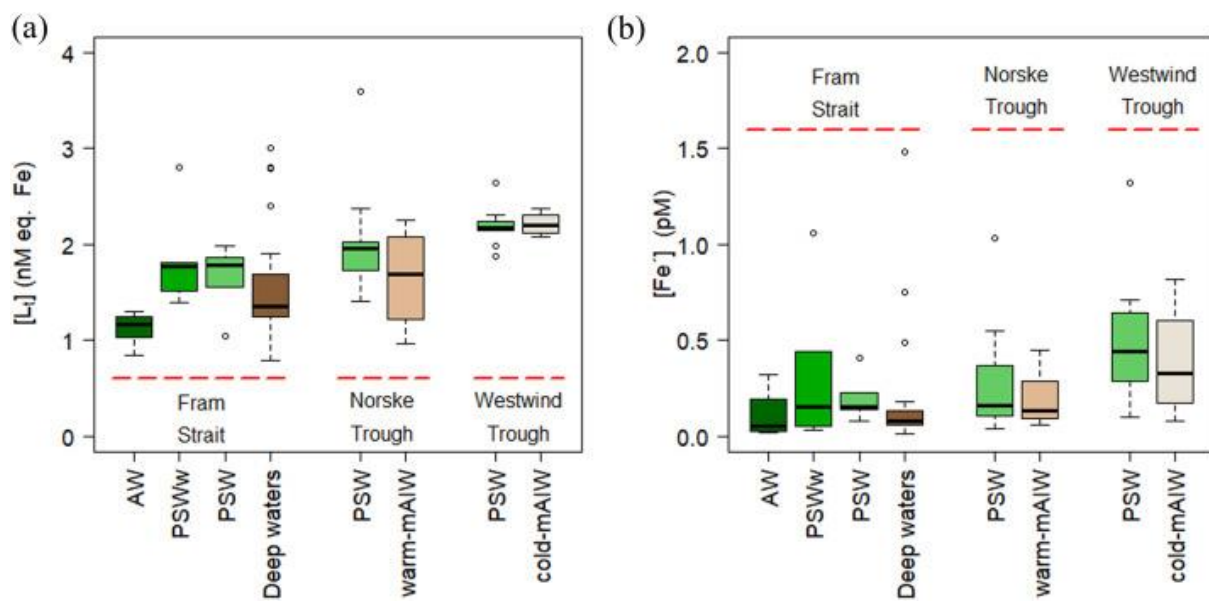
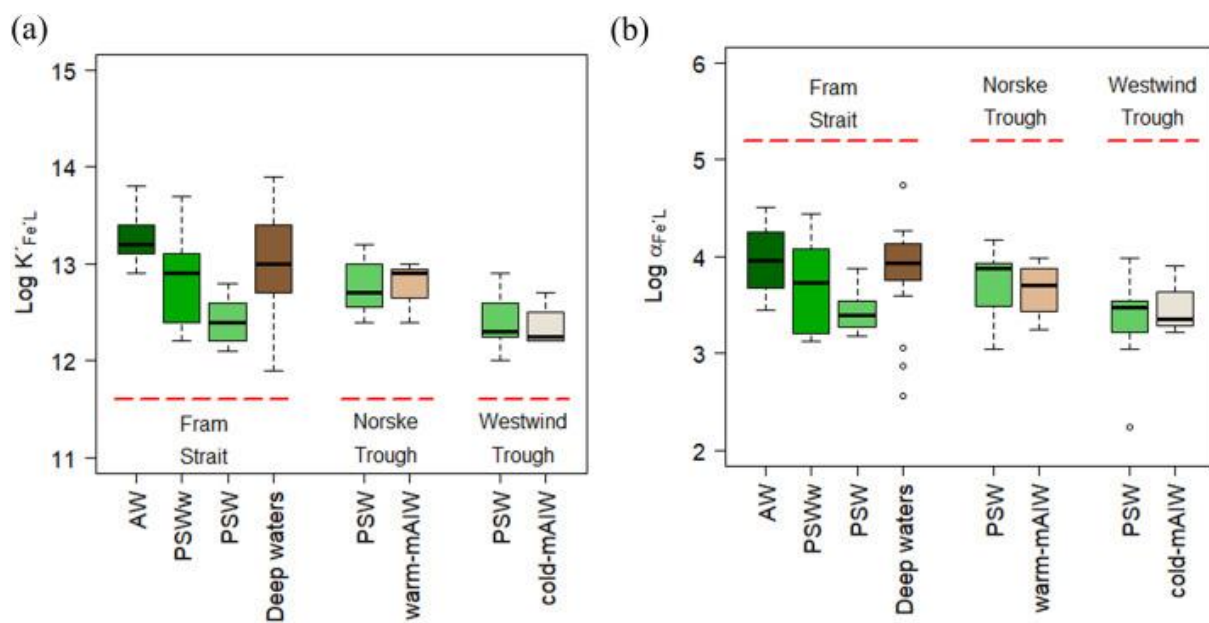


Fig. 6



Supplementary Information (SI):

Data can be accessed at : <https://doi.org/10.25850/nioz/7b.b.u>

Table 1. Values for dissolved-Fe analyses of reference materials. The consensus values were obtained from <http://www.geotraces.org/>.

	Reference Material	Consensus value	Reported value
Entire PS100/GN05 trace metal samples analyses at GEOMAR	SAFe S (#273)	0.093 ± 0.008 nM	0.101 ± 0.016 nM (n = 10)
	GSP (#144, #192)	0.27 ± 0.05 nM	0.28 ± 0.07 nM (n = 11)
Dissolved-Fe samples from ligand bottles analyses at NIOZ	SAFe D1 (#169)	0.670 ± 0.04 nM	0.718 ± 0.024 nM (n = 3)

Table 2. The summary of ligand data grouped by water mass.

Province	Water mass		$[L_t]$ (nM eq. Fe)	$\log K'_{FeL}$	$[Fe']$ (pM)	$\log \alpha_{FeL}$	$[L_t]/DFe$
Fram Strait	AW	Mean	1.15	13.3	0.08	3.5	2.0
		SD	0.18	0.3	0.11	1.5	1.0
		N	8	8	7	8	8
		Median	1.20	13.3	0.05	4.0	2.0
	PSW _w	Mean	1.84	12.9	0.31	3.7	2.4
		SD	0.50	0.6	0.39	0.5	1.2
		N	6	6	6	6	6
		Median	1.77	12.9	0.15	3.7	2.2
	PSW	Mean	1.63	12.6	0.18	3.6	3.1
		SD	0.33	0.5	0.13	0.4	1.0
		N	6	6	6	6	6
		Median	1.67	12.5	0.14	3.5	2.8
	deep waters	Mean	1.59	13.0	0.21	3.7	2.5
		SD	0.65	0.6	0.36	0.8	1.3
		N	20	20	19	20	20
		Median	1.36	13.0	0.08	3.9	2.1
Norske Trough	PSW	Mean	2.03	12.8	0.28	3.7	2.3
		SD	0.58	0.3	0.30	0.4	0.9
		N	11	11	11	11	11
		median	1.96	12.7	0.16	3.9	2.0
	warm-mAIW	Mean	1.65	12.8	0.11	3.7	2.6
		SD	0.55	0.3	0.04	0.3	1.3
		N	4	4	3	4	4
		Median	1.68	12.9	0.13	3.7	2.6
Westwind Trough	PSW	Mean	2.19	12.4	0.48	3.3	1.9
		SD	0.19	0.3	0.34	0.4	0.4
		N	11	11	10	11	11
		Median	2.17	12.3	0.41	3.5	1.9
	cold-mAIW	Mean	2.21	12.4	0.39	3.5	2.7
		SD	0.13	0.2	0.31	0.3	0.8
		N	4	4	4	4	4
		Median	2.20	12.3	0.33	3.4	2.9

Table 3. T-test statistics summary. The significance levels are $p < 0.005^{***}$, $p < 0.01^{**}$, $p < 0.05^*$ and $p < 0.1$.

		Parameters	P-value	
Fram Strait	AW vs PSW	[L _i]	0.03	*
		log K'_{FeL}	0.0009	***
		log α_{FeL}	>0.1	
	AW vs PSWw	[L _i]	0.015	*
		log K'_{FeL}	>0.1	
		log α_{FeL}	>0.1	
Northeast Greenland shelf	PSW in the Norske Trough vs. PSW in the Westwind Trough	[L _i]	0.008	**
		log K'_{FeL}	0.009	**
		log α_{FeL}	0.032	*
	mAIW in the Norske Trough vs. mAIW in the Westwind Trough	[L _i]	0.095	
		log K'_{FeL}	0.042	*
		log α_{FeL}	>0.1	

Note: the bold emphasis is mentioned in the discussion, and the others are provided as reference.

Fig. S1

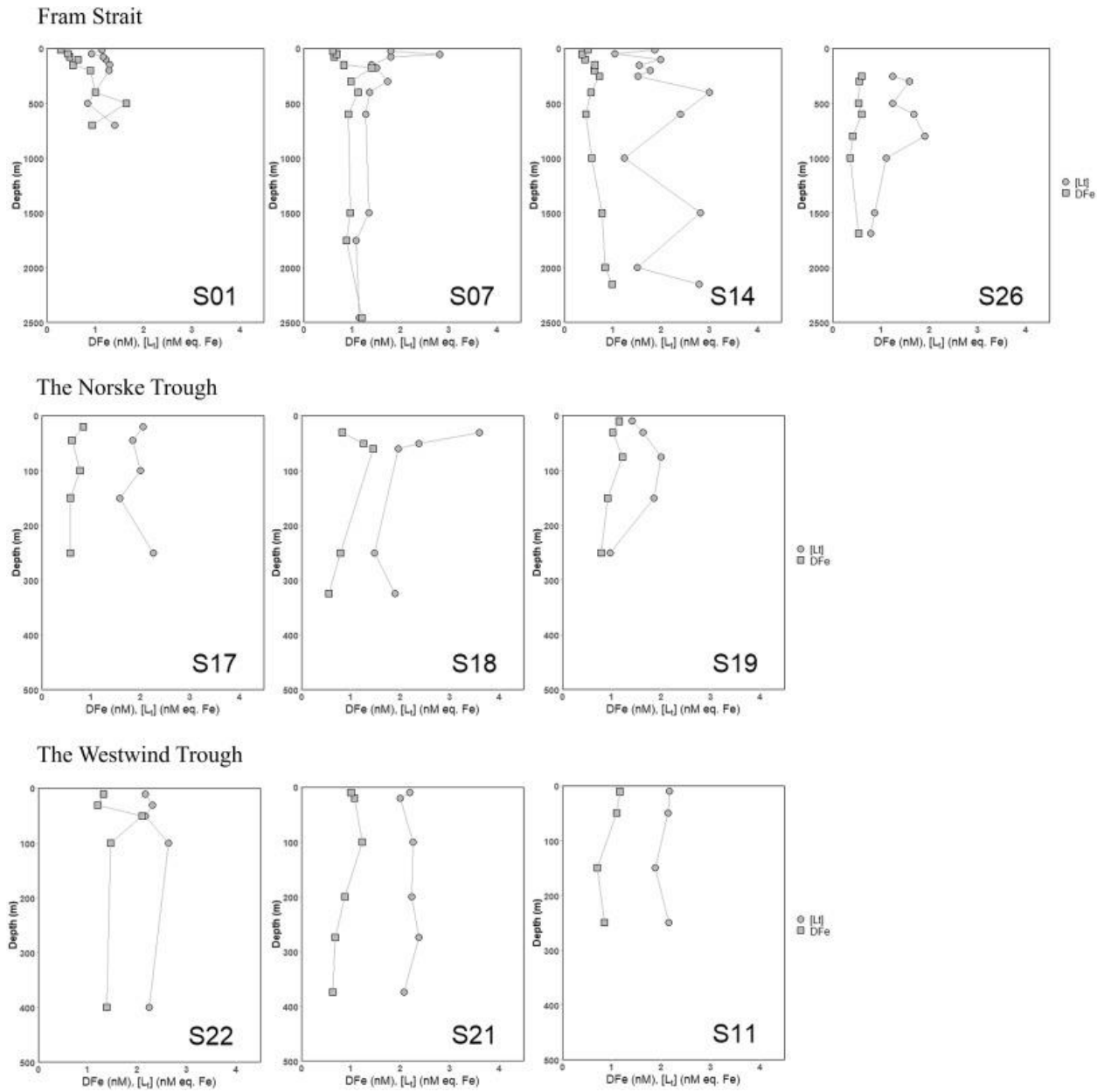


Fig. S2

